International Journal of Greenhouse Gas Control 89 (2019) 1–8

Contents lists available at ScienceDirect

International Journal of Greenhouse Gas Control

journal homepage: www.elsevier.com/locate/ijggc

Demonstrating the potential of CO_2 hydrate self-sealing in Svalbard, Arctic Norway

Stian Almenningen[a,*], Peter Betlem[b], Arif Hussain[c], Srikumar Roy[c], Kim Senger[b], Geir Ersland[a]

[a] Department of Physics and Technology, University of Bergen, PO Box 7809, 5020, Bergen, Norway
[b] Department of Arctic Geology, University Centre in Svalbard, PO Box 156, 9171, Longyearbyen, Norway
[c] iCRAG, School of Earth Sciences, University College Dublin, Belfield, D04N2E5, Ireland

ARTICLE INFO

Keywords:
CCS in Longyearbyen, Norway
CO_2 hydrate formation
Extra (secondary) sealing

ABSTRACT

Here we report the potential self-sealing properties of CO_2 hydrate for the Longyearbyen CO_2 Lab's shallow aquifer in Svalbard, Arctic Norway, through hydrate formation experiments. The experiments were conducted on a 9 cm long core plug of a fluvio-deltaic sandstone of the Barremian Helvetiafjellet Formation recovered from a fully-cored research well in Adventdalen in Svalbard at a depth of 187 m. CO_2 injection into the brine-filled (1.0 wt.% NaCl) core plug was conducted at realistic reservoir conditions; the pore pressure was 20 bar and the temperature was 0.1 °C. Solid CO_2 hydrate formed in the core plug after injecting 0.40 pore volumes (frac.) of CO_2 and immediately reduced the apparent permeability to zero. A differential pressure across the core plug of 18 bar (200 bar/m) was sustained for 250 h without producing any CO_2 from the core plug. This demonstrates the potential of CO_2 hydrate formation as a secondary seal in settings with favorable CO_2 hydrate formation conditions in or above the reservoir. The results further indicate that the self-sealing nature of CO_2 hydrate should be considered while characterizing carbon sequestration reservoirs in both marine and permafrost-affected settings.

1. Introduction

Geological sequestration of anthropogenic CO_2 is acknowledged as an important contribution to mitigate the increase of global mean temperatures (IPCC, 2014). Different options exist for storing CO_2 in the subsurface: storage in depleted hydrocarbon reservoirs and salt caverns, oil displacement in reservoirs, displacement of methane and sequestration in coal beds, and storage in deep saline aquifers (Bachu, 2000). Injection of CO_2 into oil reservoirs has been used for decades to enhance the oil recovery (Blunt et al., 1993), providing an economic incentive for energy companies to inject and store CO_2. The largest potential of CO_2 sequestration in geological media is found in deep saline aquifers (Bachu, 2015), and several projects have already been initiated (Michael et al., 2010; Eiken et al., 2011). For instance, one million tons of liquid CO_2 separated offshore from a CO_2-rich produced gas are injected annually into the Utsira aquifer 800 m below the seabed in the northern North Sea (Baklid et al., 1996; Arts et al., 2008).

Sequestration of CO_2 in aquifers is not limited to geological formations offshore. Pilot-scale projects, where limited volumes of CO_2 were sequestered, were operated at, for instance, Ketzin in Germany (Kempka et al., 2010) and at Frio in Texas (Doughty et al., 2008). However, negative public opinion, concerns about groundwater contamination and NIMBY (not-in-my-backyard) opposition hamper large-scale onshore CO_2 sequestration, especially in Europe. Sub-permafrost CO_2 storage was envisioned on the Arctic archipelago of Svalbard, Norway (Braathen et al., 2012; Senger et al., 2015). The location is suitable given sedimentary successions directly beneath the settlement of Longyearbyen and the proximity to the coal-fueled power plant emitting approximately 70,000 tons of CO_2 annually (Senger et al., 2015). The main target aquifer comprises a 300 m thick sequence of tight, naturally fractured sandstones interbedded with siltstones and shales, where injectivity is ensured through fracture flow (Ogata et al., 2012; Mulrooney et al., 2019). The required storage capacity is limited compared to the expected storage capacity of the reservoir, given the modest CO_2 emissions from the power plant. Senger et al. (2015) estimated the volumetric capacity of low density CO_2 (61.15 kg/m^3) to be 0.004–3.9 million tons and high density CO_2 (807.76 kg/m^3) to be 0.052–52 million tons. The large volumetric difference is a function of different scenarios and the uncertain CO_2 phase dominated by the pressure conditions in the target reservoir. The storage aquifer is overlain by approximately 400 m of shale-dominated successions that provide sealing to the injected CO_2. The top seal integrity is evident

* Corresponding author.
E-mail address: stian.almenningen@uib.no (S. Almenningen).

https://doi.org/10.1016/j.ijggc.2019.06.010
Received 11 April 2019; Received in revised form 12 June 2019; Accepted 12 June 2019

Nomenclature

L	Core length (frac.)
P	Absolute pressure (bar)
PV	Pore volumes (frac.)
S_H	Saturation of hydrate (%)
t	Time (hours)
T	Temperature (°C)
T_2	Time constant for the decay of transverse magnetization (ms)
ΔP	Differential pressure across the core plug (bar)
Φ	Porosity (%)

from a large pressure differential across the cap rock, with hydrostatic to slightly overpressure within the overlying Helvetiafjellet Formation and severe underpressure in the lower part of the cap rock and the underlying reservoir sandstones (Senger et al., 2016; Birchall et al., 2018). Decompaction fracturing related to Cenozoic uplift and enhanced by periodic glaciations and deglaciations is considered the main contributor to the underpressure. The seal comprises the Lower Cretaceous Rurikfjellet Formation composed of shales intercalated with thin sandstone beds, and the Upper Jurassic-Lower Cretaceous Agardhfjellet Formation consisting of organic-rich, fossiliferous, shaly successions (Koevoets et al., 2018). The presence of natural thermogenic gas within the lower, most organic-rich part of the Agardhfjellet Formation suggests that "shale gas" may occur regionally. In places where the Agardhfjellet Formation lies within the gas hydrate stability zone (Betlem et al., 2019), this may lead to gas hydrate formation within the fracture systems of the shales. An upper aquifer, comprising the fluvial-dominated sandstones of the Lower Cretaceous Helvetiafjellet Formation (Grundvåg et al., 2019), serves as a possible test site for injection of gas-phase CO_2 in the shallow subsurface, as well as a possible monitoring layer immediately beneath the permafrost. In this study, we utilize a core plug from this upper aquifer.

Successful implementation of subsurface carbon storage relies on a geological seal that traps injected CO_2, but it has been advocated that CO_2 hydrate formation in the subsurface may immobilize upward migrating CO_2 that has leaked through a stratigraphic or structural trap (Koide et al., 1995, 1997). CO_2 hydrate consists of a lattice of water molecules arranged around a CO_2 guest molecule, and the solid compound is known to reduce permeability when forming inside a porous rock (Almenningen et al., 2019; Kleinberg et al., 2003). The concept of CO_2 immobilization by hydrate formation has been proven under laboratory conditions for Bentheim sandstone core plugs (Gauteplass et al., 2018) and in unconsolidated sand (Tohidi et al., 2010), showing the potential for CO_2 hydrate self-sealing in carbon sequestration offshore. In this paper, we investigate the same potential of CO_2 hydrate self-sealing in tight, consolidated rock from an onshore sub-permafrost setting. CO_2 hydrate formation is studied inside a core plug retrieved from the Lower Cretaceous Helvetiafjellet Formation overlying the proposed main seal in the CO_2 storage project in Longyearbyen. The 70 m thick, sandstone-dominated formation is located 100–200 m below the surface and lies partly within the permafrost region (Braathen et al., 2012), and overlaps with the estimated stability zone for both CO_2 and natural gas hydrates (Betlem et al., 2019). With theoretical conditions deemed suitable for CO_2 (and natural gas) hydrate formation, the aim of this work is to verify CO_2 hydrate formation at given reservoir conditions and demonstrate the self-immobilizing properties of CO_2 in this geological setting.

2. Experimental

2.1. Core plug analysis

The host sediment for the CO_2 injection was retrieved from well DH4 drilled in Adventdalen near Longyearbyen (Braathen et al., 2012). The cylindrical core plug with a diameter of 6.2 cm and length of 9 cm was recovered from a depth interval of 186.55–186.65 m in the Helvetiafjellet Formation. The local temperature was measured at 0.1 °C, while the local pressure is assumed to be near hydrostatic to slightly overpressured (Bælum et al., 2012). Fluid discharge analysis from a nearby pingo indicates salinity values of down to 0.5 wt.% NaCl (Hodson et al., 2019) in the upper sub-permafrost aquifer located close to the core interval. However, given the reservoir's coastal proximity, salinities of up to 3.5 wt.% NaCl are feasible, and salinity values of 1.0 wt.% NaCl were assumed for the experiments. The thermobaric conditions are favorable to CO_2 hydrate formation regardless of the salinity (Fig. 1).

The diameter of the core was reduced to 5.12 cm at the laboratory and the core was dried at 70 °C for 24 h to remove water from the pore space. The core plug was then purged under vacuum and re-saturated with brine containing 1.0 wt.% NaCl. The core was further pressurized to 60 bar with brine, and the absolute permeability was measured by constant volumetric flow rate injection and application of Darcy's law. Injection of several pore volumes of brine ensured that residual salt

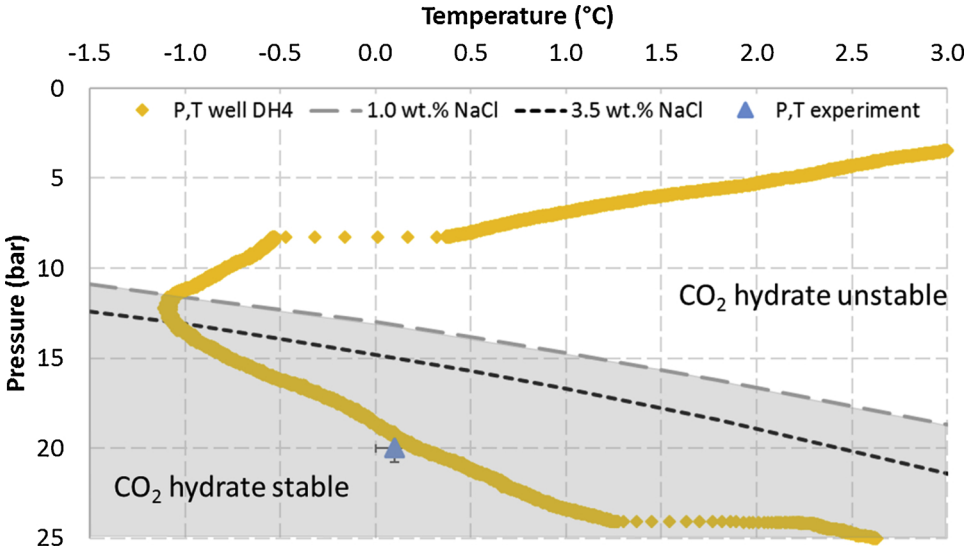

Fig. 1. Pressure and temperature (P,T) trace of well DH4. The experimental conditions (blue triangle) mimicked the actual P,T of the well at the depth interval where the core was retrieved from. The P,T conditions are favorable for CO_2 hydrate formation even at a pore-water salinity of 3.5 wt.% NaCl (similar to seawater). A salinity of 1.0 wt.% NaCl was used in the experiments in this work. The CO_2 hydrate stability curves are calculated with the CSMGem software (Colorado School of Mines, 2015).

potentially present after drying the core was displaced. The porosity was calculated by quantifying the mass of water that entered into the dry core. Magnetic resonance (MR) imaging (Bruker Biospec, 4.7 T) of the core plug saturated with water (the core plug was depressurized after the permeability measurement) provided spatial information on the initial water saturation. Standard spin-echo protocols, RAREst and MSME, were used for imaging and to provide local T_2 distributions, respectively (Mitchell et al., 2013). The spatial resolution of the images was 0.5 × 0.5 × 10 mm. Polished thin-sections and mm-scale rock chips were prepared from a neighboring core retrieved from the same well at a depth interval of 185.90–185.95 m. A blue dye was injected for porosity visualization and thin-sections were observed under Nikon Eclipse petrographic microscope to determine sandstone composition and texture. A Hitachi TM 3030Plus tabletop scanning electron microscope (SEM) fitted with Oxford EDS detector was also used for semi-quantitative elemental analysis. SEM was used consecutively to determine 3D pore structure and distribution of cemented phases (clays and quartz overgrowths) in pores. Element concentration maps were produced using the Oxford Instruments Aztec One (v.3.2) software.

2.2. Experimental set-up

A Hassler core holder connected to high-pressure pumps (ST Stigma 1000) was used to conduct the CO_2 injection experiments (Fig. 2). Separate pumps labelled injection and production were connected to each end of the core holder and facilitated injection of CO_2 and production of CO_2 and/or water. The overburden pressure was exerted by synthetic oil pressurized by a Teledyne Isco syringe pump. A rubber sleeve separated the core from the confinement oil and ensured that injected fluids passed through the interior of the core. A fixed end-piece with distribution grooves was connected to the inlet end of the core while an adjustable end-piece was used at the outlet end. The adjustable end-piece was pushed against the core end by the confinement oil and provided triaxial (radial and longitudinal) overburden pressure. Resistance measurements were enabled by an LCR meter (Hewlett-Packard) that was connected to electrodes attached to each of the two flow lines. Temperature control was provided by a refrigerator bath (Neslab RTE17) that circulated cooled antifreeze through a cooling jacket fitted outside the core holder. A temperature sensor (Omega) placed at the inlet core surface was used to monitor the temperature, and pressure readings were measured in each of the pumps.

2.3. Experimental procedure

The brine-saturated core was fitted inside the rubber sleeve and placed inside the core holder. The production pump, filled with brine, was used to pressurize the pore pressure to 20 bar while the overburden pressure simultaneously was pressurized to 50 bar. The temperature was set to 0.1 ± 0.1 °C and kept constant throughout the entire experiment. Gaseous CO_2 (> 99.999%) was injected by the injection pump from the inlet side of the core. The injected volumetric flow rate was initially 5 mL/min but was reduced to 0.1 mL/min after 30 min because of low injectivity. The production pump was set to constant pressure mode and produced the displaced water at constant pressure 20 bar. The differential pressure (injection pressure minus production pressure) and the resistance across the core were measured continuously to identify potential plugging due to CO_2 hydrate formation. A frequency of 10 kHz was used for resistance measurements, and the resistance values were later converted to resistivity by adjusting for the cross-sectional area and length of the core.

In the case of complete plugging of the core because of CO_2 hydrate formation, the long-term integrity of the hydrate plug was tested by applying a differential pressure across the core for ten days. The constant volumetric flow rate injection was then switched to constant pressure injection. A designated valve in the production flow line was used to sample the produced brine for CO_2. The core was shut-off from the production line during sampling and the brine in the production pump was depressurized into an inverted volumetric flask filled with water. Potential CO_2 in the production pump could then be quantified as gas bubbles in the volumetric flask. The production pump was re-pressurized with brine and connected back to the core after CO_2 sampling. The CO_2 hydrate plug was eventually dissociated by increasing the core temperature to room temperature while applying constant pressure. The amount of liberated CO_2 gas during dissociation was quantified and used to estimate the saturation of the hydrate plug. A hydration number of 6.2 was assumed for the CO_2 hydrate (Udachin et al., 2001).

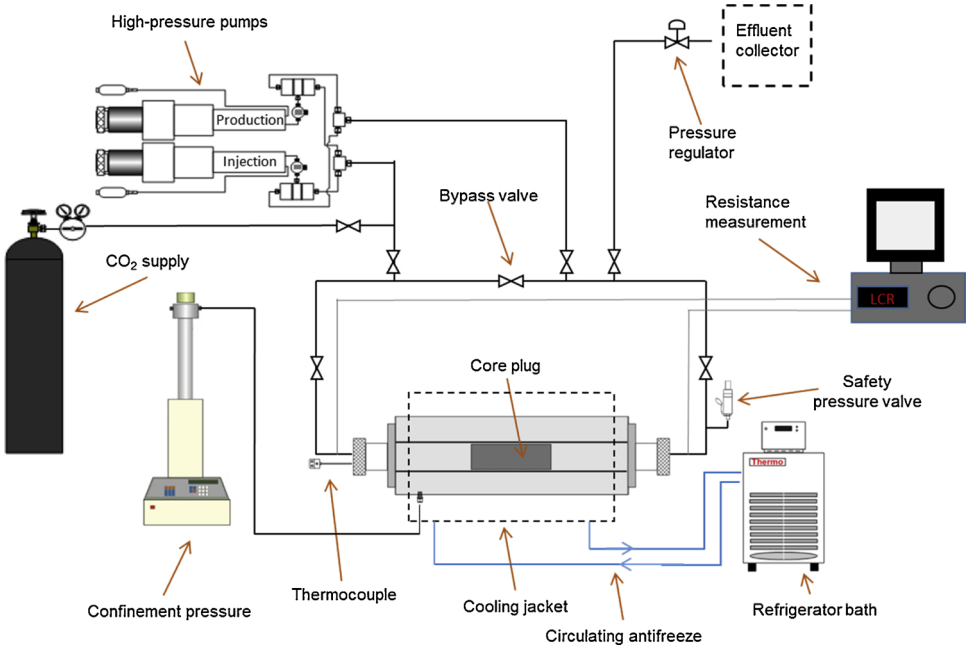

Fig. 2. Schematic of experimental design including core holder, high-pressure pumps, refrigerator bath, and LCR meter. Modified from Hågenvik (2013).

3. Results and discussion

3.1. Core plug properties

The core sample retrieved from the Helvetiafjellet Formation consisted of well-sorted, medium-grained, quartz-arenite sandstone. The quartz grains were rounded to sub-rounded and dominantly monocrystalline, with no significant fluid inclusion features (Fig. 3a and b). Most of the quartz grains exhibited undulose extinction, which was related to grain-to-grain contacts. The sandstone was quartz-cemented and showed well-developed syntaxial overgrowths (Fig. 3d) which may act as primary barrier to fluid flow. The sample was clay-poor (< 3% clay matrix), however a small proportion of dark brown to black, moderately compacted sedimentary shale fragments were observed. The shale fragments indicated ductile deformation and may occasionally block the pore space. The porosity was dominantly intergranular, with limited secondary grain dissolution porosity. Scattered rare traces of diagenetic framboidal pyrite were also observed.

The SEM-EDS results were consistent with petrographic observations and showed that the core was predominantly composed of Si (35.5 wt.%) with a very nominal contribution (< 1%) from phyllosilicate minerals, *i.e.* Al (0.3 wt.%) and K (0.1 wt.%). The concentration of other important sandstone forming minerals, like Fe, Mg, and K, was very low (perhaps below detection limit of the EDS detector) and was indicative of an overall quartzitic nature of the Helvetiafjellet Formation.

The porosity of the core plug was measured to 5.6 ± 0.1%, with an average grain density of 2.61 g/cm^3 and average grain size of 395 µm. The absolute permeability to water was measured to 0.04 ± 0.01 mD, in line with previous studies of the interval, *e.g.* Bjørlykke et al. (1979). The initial distribution of water was visualized by MR imaging (Fig. 4). The gray-scale images represent porosity maps since the core was assumed completely filled with water. The center of the middle parts of the core was lacking water compared with the rest of the core because of lower porosity in that area. The average T_2 and the area under the T_2 distribution were lower in the middle parts of the core indicating tighter pores here. Heterogeneities were also observed within the same cross-section of the core (L = 0.06, Fig. 4). The T_2 distribution was obtained for three different areas in this cross-section and showed significant discrepancies. One area (blue circle, Fig. 4) had a large intensity with an average T_2 of 2.9 ms. This area corresponds to one of the heterogeneities that is observed at the top of the core plug in Fig. 4c. These features were lithic conglomerates consisting primarily of mudstone filled with brine. The short relaxation time measured in these features reflects the small grain sizes of mudstone. A second area (red circle, Fig. 4) representing the main sandstone had a low intensity with an average T_2 of 8.4 ms. The subsequent CO_2 injection was not aided by *in situ* imaging of the core, but an unstable displacement of water by CO_2 was expected because of the unfavorable mobility ratio between CO_2 and water and the heterogeneous nature of the core plug.

3.2. Initial CO_2 hydrate plug

The initial CO_2 injection with constant volumetric rate equal to 5.0 mL/min led to an immediate increase of the injection pressure because of the low permeability of the core plug (Fig. 5). The injection rate was subsequently reduced to 0.1 mL/min, but the differential pressure (injection pressure minus production pressure) continued to increase as only 0.01 mL/min of water was being produced at the current differential pressure. The production rate increased slowly as the injection pressure increased, and the CO_2/water front arrived at the inlet core end after 6 h of injection. The low permeability of the core and corresponding low flow rate ensured that the temperature of the core was maintained at constant T = 0.1 ± .1 °C throughout the injection process. Additional four hours of CO_2 injection were sustained, equivalent of displacing 0.40 PV (frac.) of water by CO_2, before the CO_2 hydrate plug formed and abruptly diminished the flow through the core plug. The CO_2 hydrate formation was concurrently verified by no water production, increase in differential pressure, and increase in resistivity across the core plug (Fig. 5). The resistivity equipment malfunctioned during the first ten hours of the injection, but the resistivity was obtained immediately prior to and during hydrate plugging. The abrupt increase in resistivity across the length of the core verified conversion of liquid water to solid CO_2 hydrate inside the core plug. A CO_2 hydrate

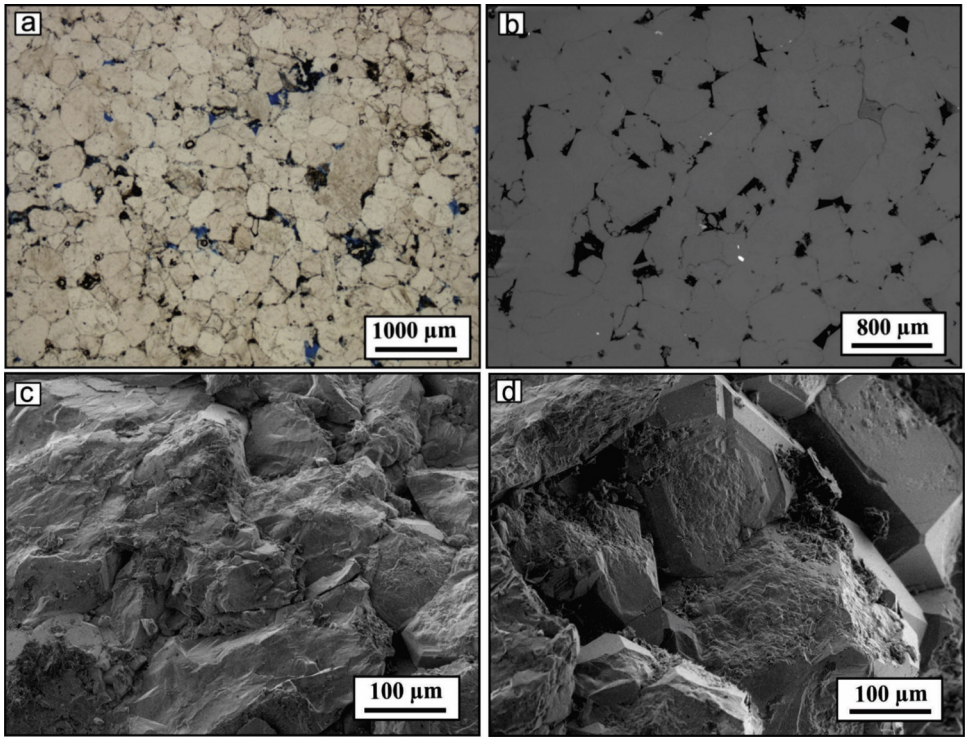

Fig. 3. a) Plane-polarized light photomicrograph of a thin-section from the lower part of the Helvetiafjellet Formation. The rock consisted of clean, well-sorted, medium-grained quartz arenite. b) BSE image showing the quartz-rich nature of the rock. The black spaces correspond to intergranular porosity whereas scattered white spots show framboidal pyrite. c) Pore-scale image of sandstone with d) well-developed syntaxial quartz overgrowths.

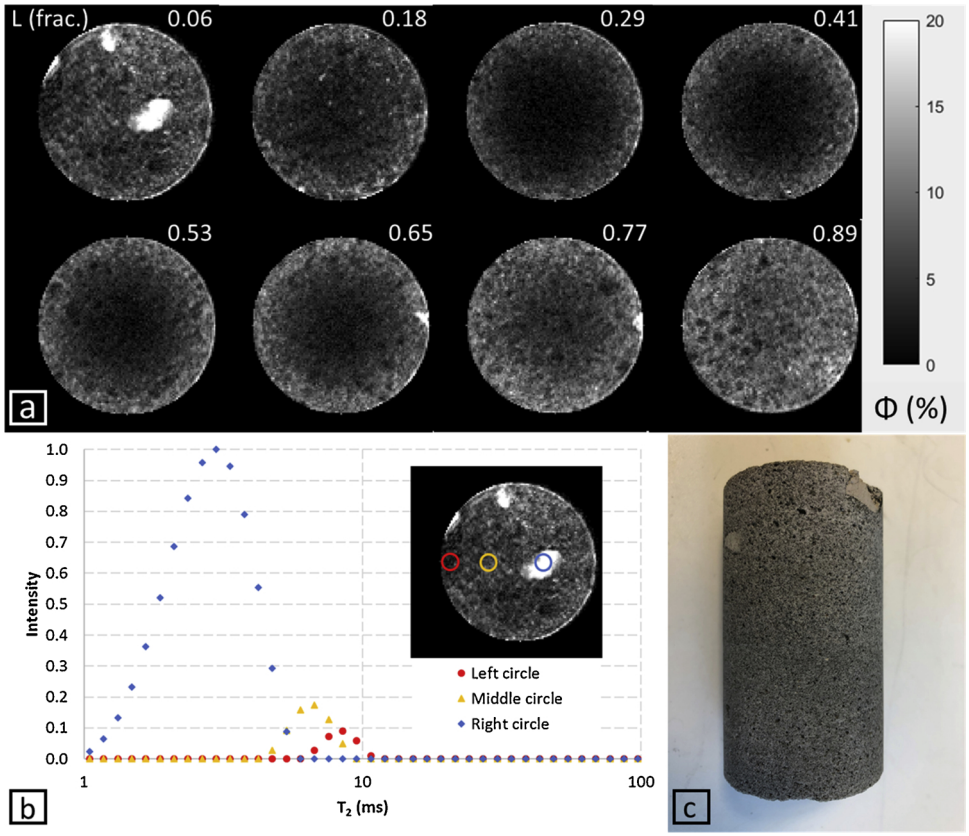

Fig. 4. a) Porosity map in gray-scale of eight different cross-sections of the core acquired from MR imaging. b) T_2 distributions from three different areas in the same cross-section of the core. Each intensity value is scaled to the peak intensity of the right area (blue diamonds). c) Photograph of the core plug.

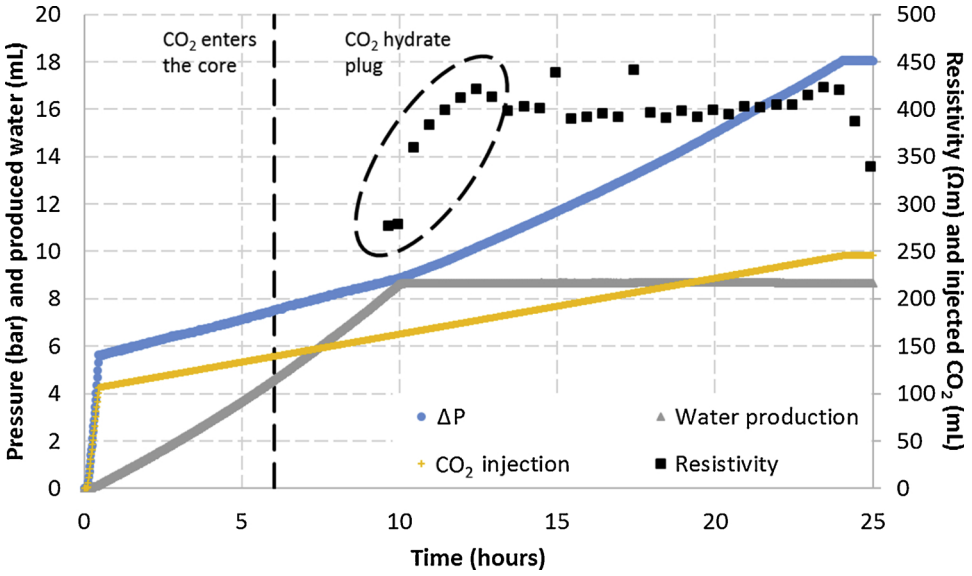

Fig. 5. Formation of CO_2 hydrate plug during CO_2 injection into water-filled core at T = 0.1 °C and P = 20 bar. The injected CO_2 was quickly pressurized to 26 bar (ΔP = 6 bar) and the differential pressure (blue circles) continued to increase as the CO_2 was injected with constant volumetric rate equal to 0.1 mL/min (yellow pluses). The injected CO_2 entered the core after 6 h, and a CO_2 hydrate plug formed after 0.40 PV (frac.) of CO_2 was injected into the core at t = 10 h. The formed CO_2 hydrate plug abruptly ended the water production (gray triangles) and increased the resistivity across the core (black squares).

plug forming only in the flow line or in the inlet end-piece contacting the core end would on the contrary not affect the resistivity measurements across the core plug.

The stability pressure of CO_2 hydrate at $T = 0.1$ °C in equilibrium with 1.0 wt.% NaCl water is 13.2 bar according to the CSMGem software (Colorado School of Mines, 2015). The initial pore-water pressure of 20 bar was already within the hydrate stability region, however, the CO_2 hydrate did not form until after four hours of CO_2 flow in the core. This time period between the moment at which the P,T conditions of hydrate formation is reached until hydrate growth begins is called the induction time. The induction time could vary stochastically from one hydrate formation to another (Sloan and Koh, 2008). In this particular CO_2 injection scheme, the CO_2 hydrate formed and plugged the flow path through the core before CO_2 broke through at the production side of the core. A core with length close to 9 cm was sufficient to produce a layer of impermeable CO_2 hydrate that effectively stopped the CO_2 from reaching the production pump. Similar CO_2 injection experiments on Bentheim sandstone resulted in the formation of CO_2 hydrate plugs, but usually the CO_2 hydrate plug formed at a later stage of the injection after CO_2 broke through the end of the core (Gauteplass et al., 2018).

Bentheim sandstone consists of more than 95% quartz (Ramstad and Rueslåtten, 2013) and has a porosity and permeability of 23–24% and 1.1–1.9 D, respectively (Almenningen et al., 2019). The lower permeability and tighter pores of the core plug from Helvetiafjellet Formation used in this study are likely to have led to more effective CO_2 hydrate sealing and a lower induction time.

The CO_2 was injected with constant volumetric rate of 0.1 mL/min for close to 15 h after the CO_2 hydrate plug formed (t = 25 h, Fig. 5), which increased the injection pressure to 38 bar. The CO_2 injection was then switched to constant pressure control, while the production pressure was kept constant to 20 bar. The induced differential pressure of 18 bar was maintained for close to 250 h to investigate the long-term stability of the CO_2 hydrate plug (Fig. 6). Neither was water produced nor CO_2 injected during this time span. The production pump was sampled twice for CO_2 after 100 and 250 h, but no CO_2 was found in the production water. The resistivity declined monotonically during the no-flow period, and may be attributed to CO_2 dissolving in the pore water with subsequent formation of carbonic acid and dissociation into conducting ions. However, adding conductive ions from CO_2 dissolution is expected to decrease the brine conductivity for high salt concentrations (Börner et al., 2015). Redistribution of the formed hydrate phase may also have an impact on the conductivity by affecting the tortuosity of the conducting brine (Hauge et al., 2016).

3.3. Second CO_2 hydrate plug

The successful CO_2 hydrate self-sealing at 20 bar was followed by a sensitivity analysis of the effect of pore pressure. The existing CO_2 hydrate plug was dissociated by reducing the injection and production pressure to 11 and 5 bar, respectively. The displacement of water by CO_2 was resumed (Fig. 7), and eventually the CO_2 broke through the core and water production was replaced by CO_2 production. After 20 h, the injection and production pressure were increased to 18 and 10 bar, respectively. The injected CO_2 was pressurized above the hydrate stability pressure of 13.2 bar, and the pressure dropped linearly through the length of the core plug to the production pressure below the hydrate stability pressure. The CO_2 flow remained constant for 20 h during this pressure condition and no CO_2 hydrate formed. The pressure was then further increased to 20 bar for the injection pressure and 15 bar for the production pressure. This led to an immediate formation of CO_2 hydrate and the pore space was again blocked for CO_2 flow. The CO_2 hydrate formed a flow barrier independent of whether CO_2 displaced water in a fully water saturated core, or CO_2 flowed through already established flow channels in conjunction with residual water. The saturation history of the core was insignificant as long as the P,T conditions were favorable for hydrate formation.

The core remained plugged for 450 h and no CO_2 was injected nor produced in this time period (Fig. 8). The production pump was already filled with CO_2 by the time the hydrate plug formed and explicit CO_2 sampling was therefore not performed during the long-term stability testing. The resistivity response was similar as to the initial long-term test and showed a steady decline during the no-flow period.

Thermal stimulation through temperature increase was used to dissociate the CO_2 hydrate plug after the long-term integrity of the plug was verified (Fig. 9). The theoretical CO_2 hydrate dissociation temperature was already reached at T = 1.2 °C given the moderate overpressure at the production side, but dissociation was not observed until some minutes later when the temperature had increased to 2.3 °C. One hour later the CO_2 hydrate plug was completely dissociated and the flow of CO_2 recommenced. The amount of released CO_2 gas during the dissociation process was quantified and used to estimate the CO_2 hydrate saturation in the core as approximately, S_H = 5%. The magnitude of the CO_2 hydrate saturation had thus been small but still effective in blocking the flow through the core. The CO_2 hydrate most likely formed at the interface between CO_2 gas and residual liquid water, which has been previously observed for liquid CO_2 at higher pressure (Almenningen et al., 2018). A thin but extensive solid CO_2 hydrate layer immobilized the flow channels of gaseous CO_2. The blocking was probably most pronounced in pore throats connecting the intergranular pores (Fig. 3b).

4. Concluding remarks

The effectiveness of CO_2 hydrate self-sealing was verified in a core plug retrieved from the Helvetiafjellet Formation in Svalbard, Norway. 0.40 PV (frac.) of CO_2 was injected at reservoir P,T conditions before the flow of CO_2 was blocked by CO_2 hydrate formation. A repeated test, where initial flow of CO_2 through the core was established, also led to complete blocking of CO_2 flow when the injection and production pressure were increased above the CO_2 hydrate stability pressure. The flow of CO_2 was effectively stopped when the P,T conditions were favorable for hydrate formation, independent of whether CO_2 displaced water for the first time or CO_2 flowed in already established flow channels in conjunction with residual water. The formed CO_2 hydrate seal was impermeable for the entire length of the experiments (several hundred hours).

The core plug experiments in this work demonstrates the potential of CO_2 hydrate self-sealing as a secondary safety factor in the CCS

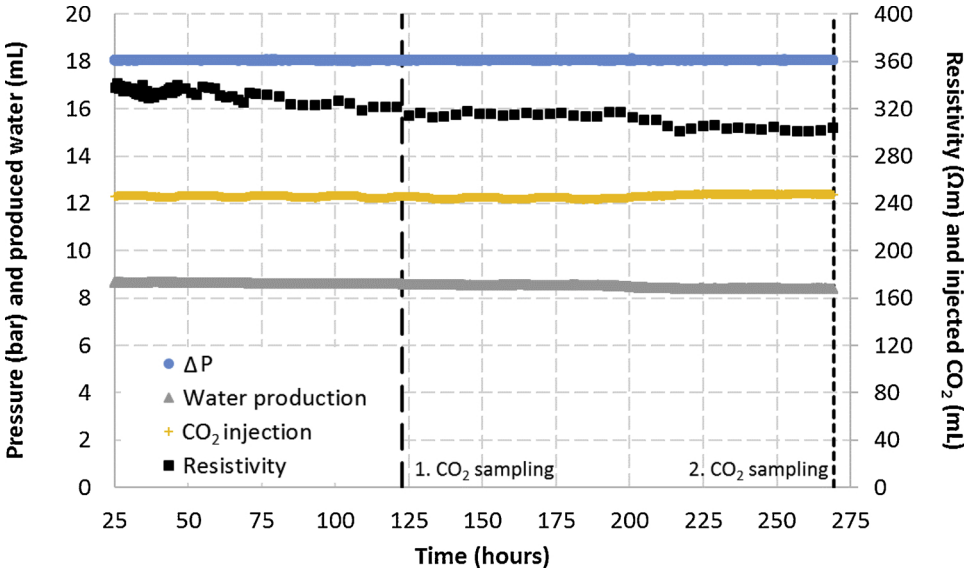

Fig. 6. Long-term stability of the CO_2 hydrate plug at T = 0.1 °C and constant differential pressure across the core equal to 18 bar (blue circles). No CO_2 was injected (yellow pluses) and no water was produced (gray triangles) during 250 h. The effluent water was sampled for CO_2 twice, but no CO_2 escaped through the hydrate-plugged core.

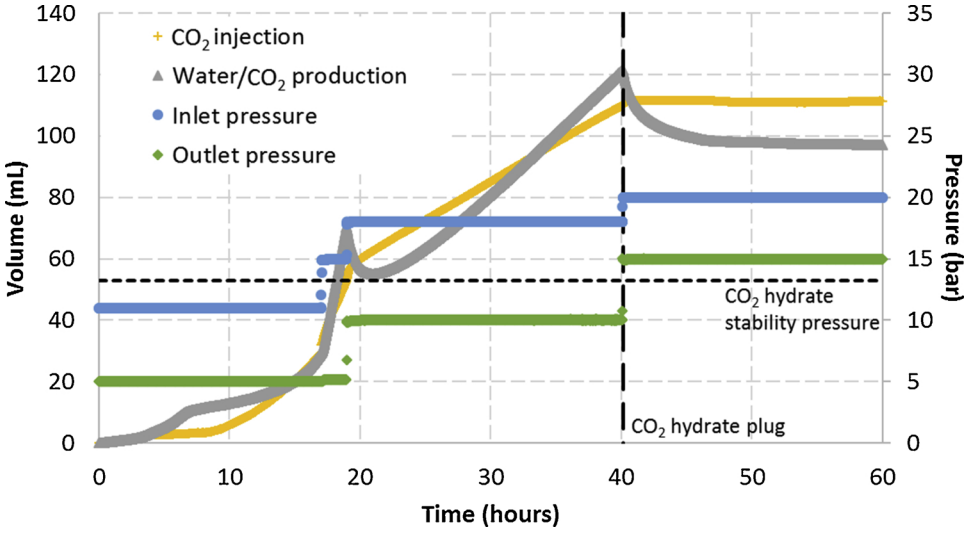

Fig. 7. Pressure-controlled CO_2 injection (yellow pluses) below and above the CO_2 hydrate stability pressure (P = 13.2 bar) at T = 0.1 °C. The flow of CO_2 through the core was sustained even when the injection pressure (blue circles) was set to 18 bar and the production pressure (green diamonds) was set to 10 bar. CO_2 hydrate plugging commenced after 40 h when the injection and production pressure were set to 20 bar and 15 bar, respectively. The CO_2 hydrate stability pressure is calculated with the CSMGem software (Colorado School of Mines, 2015).

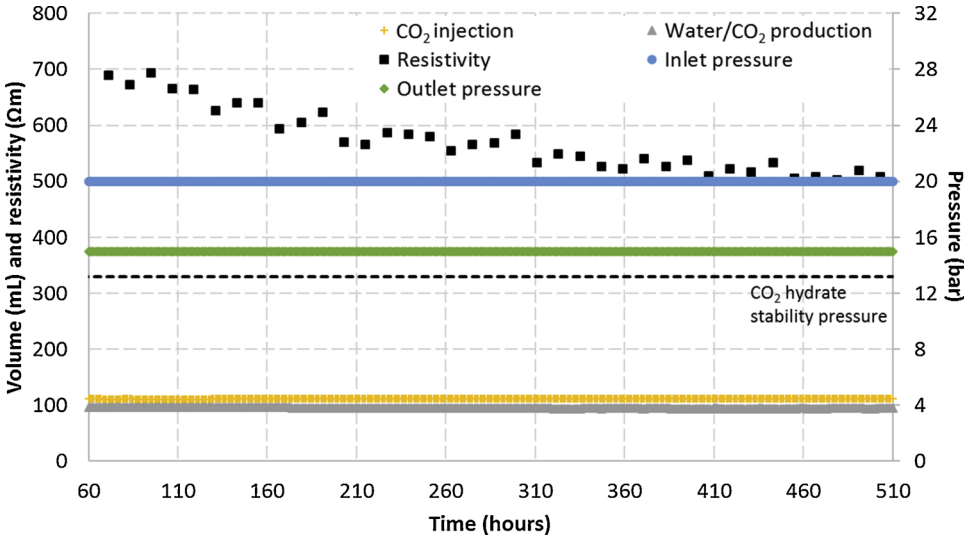

Fig. 8. Long-term stability of the CO_2 hydrate plug at T = 0.1 °C and constant differential pressure across the core equal to 5 bar. No CO_2 was injected (yellow pluses) and no water was produced (gray triangles) during 450 h. The CO_2 hydrate stability pressure is calculated with the CSMGem software (Colorado School of Mines, 2015).

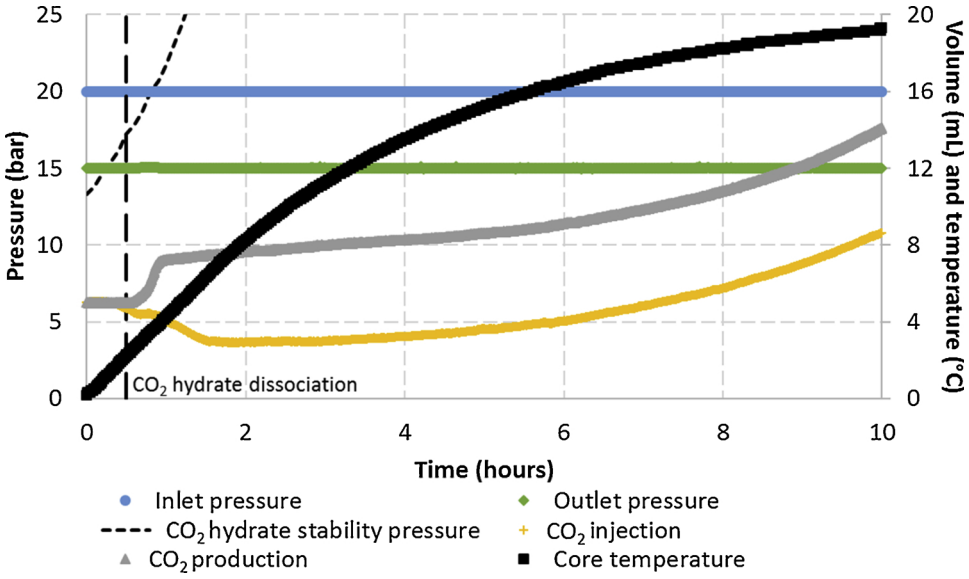

Fig. 9. Thermal dissociation of CO_2 hydrate plug at constant injection pressure (blue circles) equal to 20 bar and constant production pressure (green diamonds) equal to 15 bar. The CO_2 hydrate plug started to dissociate after 0.5 h when the temperature reached 2.3 °C (black squares). The flow of CO_2 through the core was recommenced after approximately 2 h. The CO_2 hydrate stability curve is calculated with the CSMGem software (Colorado School of Mines, 2015).

project in Longyearbyen. In the unlikely event of CO_2 leakage through the top seal overlying the CO_2 injection target, the CO_2 will react with the pore water and form hydrates at the prevailing *P*,*T* conditions in the Helvetiafjellet Formation. The results suggest that the CO_2 hydrate self-sealing is not limited to CO_2 sequestration in shallow marine aquifers, but applies as well to CO_2 storage projects in permafrost settings. The hydrate blockage of pores is more effective in low permeability rock with tight pores than in high permeability rock associated with unconsolidated sediments offshore. The long-term integrity of the formed hydrate seal cannot be determined through laboratory core plug experiments alone, and should be investigated by field-scale numerical simulations. Further, it should be considered that the hydrate seal will be prone to vertical shifts in response to changing surface temperatures, and the upward movement of the CO_2 hydrate stability zone potentially caused by global warming.

Acknowledgements

The authors would like to acknowledge Equinor for financial support and the use of the MRI facility at Equinor's laboratories in Bergen. The core sample and reservoir conditions were provided by the Longyearbyen CO_2 Lab project (http://co2-ccs.unis.no). The constructive feedback from two anonymous reviewers is much appreciated.

References

Almenningen, S., Gauteplass, J., Fotland, P., Aastveit, G.L., Barth, T., Ersland, G., 2018. Visualization of hydrate formation during CO2 storage in water-saturated sandstone. Int. J. Greenh. Gas Control 79, 272–278.

Almenningen, S., Gauteplass, J., Hauge, L.P., Barth, T., Fernø, M.A., Ersland, G., 2019. Measurements of CH4 and CO2 relative permeability in hydrate-bearing sandstone. J. Pet. Sci. Eng. 177, 880–888.

Arts, R.J., Chadwick, A., Eiken, O., Thibeau, S., Nooner, S., 2008. Ten Years' Experience of Monitoring CO2 Injection in the Utsira Sand at Sleipner, Offshore Norway. First Break, pp. 26.

Bachu, S., 2000. Sequestration of CO2 in geological media: criteria and approach for site selection in response to climate change. Energy Convers. Manage. 41, 953–970.

Bachu, S., 2015. Review of CO2 storage efficiency in deep saline aquifers. Int. J. Greenh. Gas Control 40, 188–202.

Bælum, K., Johansen, T.A., Johnsen, H., Rod, K., 2012. Subsurface structures of the Longyearbyen CO2 Lab study area in Central Spitsbergen (Arctic Norway), as mapped by reflection seismic data. Nor. J. Geol. 92, 377–389.

Baklid, A., Korbol, R., Owren, G., 1996. Sleipner vest CO2 disposal, CO2 injection into a shallow underground aquifer. SPE Annual Technical Conference and Exhibition.

Betlem, P., Senger, K., Hodson, A., 2019. 3D thermobaric modelling of the gas hydrate stability zone onshore central Spitsbergen, Arctic Norway. Mar. Pet. Geol. 100, 246–262.

Birchall, T., Senger, K., Braathen, A., Olaussen, S., 2018. Subnormal pressure regimes of the northern Barents Shelf: causes and implications for hydrocarbon exploration. EAGE Annual Conference & Exhibition.

Bjørlykke, K., Elvekhøi, B.A., Malm, A.O., 1979. Diagenesis in Mesozoic sandstones from Spitsbergen and the North Sea—a comparison. Geol. Rundschau 68, 1152–1171.

Blunt, M., Fayers, F.J., Orr, F.M., 1993. Carbon dioxide in enhanced oil recovery. Energy Convers. Manage. 34, 1197–1204.

Börner, J.H., Herdegen, V., Repke, J.U., Spitzer, K., 2015. The electrical conductivity of CO2-bearing pore waters at elevated pressure and temperature: a laboratory study and its implications in CO2 storage monitoring and leakage detection. Geophys. J. Int. 203, 1072–1084.

Braathen, A., Bælum, K., Christiansen, H.H., Dahl, T., Eiken, O., Elvebakk, H., Hansen, F., Hanssen, T.H., Jochmann, M., Johansen, T.A., Johnsen, H., Larsen, L., Lie, T., Mertes, J., Mørk, A., Mørk, M.B., Nemec, W., Olaussen, S., Oye, V., Rød, K., Titlestad, G.O., Tveranger, J., Vagle, K., 2012. The Longyearbyen CO2 Lab of Svalbard, Norway—initial assessment of the geological conditions for CO2 sequestration. Nor. J. Geol. 92, 353–376.

Colorado School Of Mines, 2015. Center for Hydrate Research. [Online]. Available: http://hydrates.mines.edu/CHR/Software.html (Accessed 2 March 2016). .

Doughty, C., Freifeld, B.M., Trautz, R.C., 2008. Site characterization for CO2 geologic storage and vice versa: the Frio brine pilot, Texas, USA as a case study. Environ. Geol. 54, 1635–1656.

Eiken, O., Ringrose, P., Hermanrud, C., Nazarian, B., Torp, T.A., Høier, L., 2011. Lessons learned from 14 years of CCS operations: Sleipner, In Salah and Snøhvit. Energy Procedia 4, 5541–5548.

Gauteplass, J., Almenningen, S., Ersland, G., Barth, T., 2018. Hydrate seal formation during laboratory CO2 injection in a cold aquifer. Int. J. Greenh. Gas Control 78, 21–26.

Grundvåg, S.E., Jelby, M.E., Sliwinska, K.K., Nøhr-Hansen, H., Aadland, T., Sandvik, S.E., Tennvassås, I., Engen, T., Olaussen, S., 2019. Sedimentology and palynology of the Lower Cretaceous succession of central Spitsbergen: integration of subsurface and outcrop data. Nor. J. Geol. http://www.arcex.no/norwegian-journal-of-geology-sedimentology-and-palynology-of-the-lower-cretaceous-succession-of-central-spitsbergen-integration-of-subsurface-and-outcrop-data/.

Hågenvik, C., 2013. CO2 Injection in Hydrate Bearing Sandstone with Excess Water. MSc. University of Bergen, Norway.

Hauge, L.P., Gauteplass, J., Høyland, M.D., Ersland, G., Kovscek, A., Fernø, M.A., 2016. Pore-level hydrate formation mechanisms using realistic rock structures in high-pressure silicon micromodels. Int. J. Greenh. Gas Control 53, 178–186.

Hodson, A.J., Nowak, A., Redeker, K.R., Holmlund, E.S., Christiansen, H.H., Turchyn, A.V., 2019. Seasonal dynamics of methane and carbon dioxide evasion from an open system Pingo: Lagoon Pingo, Svalbard. Front. Earth Sci. 7.

IPCC, 2014. R.K. Pachauri L.A. Meyer Geneva, SwitzerlandClimate Change 2014: Synthesis Report. Contribution of Working Groups I, II and III to the Fifth Assessment Report of the Intergovernmental Panel on Climate Change [Core Writing Team2014. Pachauri, R.K., Meyer, L.A. (Eds.), Climate Change 2014: Synthesis Report. Contribution of Working Groups I, II and III to the Fifth Assessment Report of the Intergovernmental Panel on Climate Change [Core Writing Team.

Kempka, T., Kühn, M., Class, H., Frykman, P., Kopp, A., Nielsen, C.M., Probst, P., 2010. Modelling of CO2 arrival time at Ketzin – part I. Int. J. Greenh. Gas Control 4, 1007–1015.

Kleinberg, R.L., Flaum, C., Griffin, D.D., Brewer, P.G., Malby, G.E., Peltzer, E.T., Yesinowski, J.P., 2003. Deep sea NMR: methane hydrate growth habit in porous media and its relationship to hydraulic permeability, deposit accumulation, and submarine slope stability. J. Geophys. Res. Solid Earth 108, 1–17.

Koevoets, M.J., Hammer, Ø., Olaussen, S., Senger, K., Smelror, M., 2018. Integrating subsurface and outcrop data of the Middle Jurassic to Lower Cretaceous Agardhfjellet Formation in central Spitsbergen. Nor. J. Geol. 98.

Koide, H., Takahashi, M., Tsukamoto, H., Shindo, Y., 1995. Self-trapping mechanisms of carbon dioxide in the aquifer disposal. Energy Convers. Manage. 36, 505–508.

Koide, H., Takahashi, M., Shindo, Y., Tazaki, Y., Iijima, M., Ito, K., Kimura, N., Omata, K., 1997. Hydrate formation in sediments in the sub-seabed disposal of CO2. Energy 22, 279–283.

Michael, K., Golab, A., Shulakova, V., Ennis-King, J., Allinson, G., Sharma, S., Aiken, T., 2010. Geological storage of CO2 in saline aquifers—a review of the experience from existing storage operations. Int. J. Greenh. Gas Control 4, 659–667.

Mitchell, J., Chandrasekera, T.C., Holland, D.J., Gladden, L.F., Fordham, E.J., 2013. Magnetic resonance imaging in laboratory petrophysical core analysis. Phys. Rep. 526, 165–225.

Mulrooney, M.J., Larsen, L., Van Stappen, J., Rismyhr, B., Senger, K., Braathen, A., Olaussen, S., Mørk, M.B.E., Ogata, K., Cnudde, V., 2019. Fluid flow properties of the Wilhelmøya Subgroup, a potential unconventional CO2 storage unit in central Spitsbergen. Nor. J. Geol. 99.

Ogata, K., Senger, K., Braathen, A., Tveranger, J., Olaussen, S., 2012. The Importance of Natural Fractures in a Tight Reservoir for Potential CO2 Storage: A Case Study of the Upper Triassic–middle Jurassic Kapp Toscana Group (Spitsbergen, Arctic Norway). Geological Society, London Special Publications, 374, SP374.9.

Ramstad, T., Rueslåtten, H., 2013. Pore Scale Numerical Analysis for Geological Sequestration of CO2. Technical Report, 1-63.

Senger, K., Tveranger, J., Braathen, A., Olaussen, S., Ogata, K., Larsen, L., 2015. CO2 storage resource estimates in unconventional reservoirs: insights from a pilot-sized storage site in Svalbard, Arctic Norway. Environ. Earth Sci. 73, 3987–4009.

Senger, K., Mulrooney, M.J., Braathen, A., Ogata, K., Olaussen, S., 2016. Integrated characterization of an organic-rich Caprock Shale, Svalbard, Arctic Norway. Fifth EAGE Shale Workshop.

Sloan, E.D., Koh, C., 2008. Clathrate Hydrates of Natural Gases. CRC Press, Boca Raton, Florida.

Tohidi, B., Yang, J., Salehabadi, M., Anderson, R., Chapoy, A., 2010. CO2 hydrates could provide secondary safety factor in subsurface sequestration of CO2. Environ. Sci. Technol. 44, 1509–1514.

Udachin, K.A., Ratcliffe, C.I., Ripmeester, J.A., 2001. Structure, composition, and thermal expansion of CO2 hydrate from single crystal X-ray diffraction measurements. J. Phys. Chem. B 105, 4200–4204.